CMS Physics Analysis Summary

Contact: cms-pag-conveners-susy@cern.ch 2015/09/13

Search for R-parity-violating supersymmetry in proton-proton collisions at $\sqrt{s}$ = 8 TeV in events with large jet and b-jet multiplicity

The CMS Collaboration

Abstract

Preliminary results are reported from a search for new physics beyond the standard model (SM) in proton-proton collisions at a center-of-mass energy $\sqrt{s} = 8$ TeV, focusing on the signature of large multiplicity of jets and b-tagged jets. The data sample comprises an integrated luminosity of 19.5 fb^{-1}, recorded by the CMS experiment at the Large Hadron Collider (LHC). The results are used to exclude gluinos with $m_{\text{gluino}} < 980$ GeV in an R-parity violating supersymmetric extension of the standard model in which each gluino decays via $\tilde{g} \to tbs$.

1 Introduction

Supersymmetry (SUSY) is an attractive extension of the standard model (SM) because SUSY can solve the hierarchy problem and ensure gauge coupling unification [1, 2]. The majority of searches for SUSY focus on R-parity-conserving (RPC) models. The R-parity of a particle is defined by $R = (-1)^{3B+L+2s}$, where B and L are its baryon and lepton numbers respectively, and s is the particle spin [3]. In RPC SUSY, the lightest superpartner (LSP) is stable, which ensures proton stability and provides a dark-matter candidate. All SM particle fields have $R = +1$; all superpartner fields have $R = -1$.

Supersymmetric models with R-parity-violating (RPV) interactions violate either B or L [4, 5]. The superpotential $W_{\rm RPV}$ includes a bilinear term proportional to the coupling μ'_i and three trilinear terms parameterized by the couplings λ_{ijk}, λ'_{ijk}, and λ''_{ijk}:

$$W_{\rm RPV} = \frac{1}{2}\,\lambda_{ijk} L_i L_j \overline{E}_k + \lambda'_{ijk} L_i Q_j \overline{D}_k \; + \; \frac{1}{2}\,\lambda''_{ijk} \overline{U}_i \overline{D}_j \overline{D}_k + \mu'_i H_u L_i, \tag{1}$$

where i, j, and k are generation indices; L, Q and H_u are the lepton, quark and up-type Higgs $SU(2)_L$ doublet superfields; and $\overline{E}$, $\overline{D}$, and $\overline{U}$ are the charged lepton, down-type quark and up-type quark $SU(2)_L$ singlet superfields. The third term violates baryon number conservation, while the first two terms violate lepton number conservation. The final term, involving the lepton and up-type Higgs doublets, is also allowed in the superpotential but the effects of this term are not considered in this analysis.

Experimental bounds on hadronic, semileptonic and leptonic R-parity-violating couplings are highly orthogonal due to the strong constraint on their magnitude from nucleon stability measurements. For example, for squark masses of 1 TeV, the absence of any observation of proton decay results in the constraint $|\lambda'_{ijk}\lambda^{\star}_{i'j'k'}| < \mathcal{O}(10^{-9})$ for all generation indices [6]. Much stronger constraints are possible for couplings involving light generations, and similar constraints exist for products of other R-parity-violating couplings.

A subset of RPV scenarios focus on the R-parity-violating extension of the minimal supersymmetric model (MSSM) when the assumption of minimal flavor violation (MFV) is imposed [7, 8]. Under this assumption, the only sources of R-parity violation are the SM Yukawa couplings, and the R-parity-violating couplings are related to the components of the Cabibbo-Kobayashi-Maskawa matrix and the fermion masses.

In RPV models the LSP is unstable, and consequently other SUSY search techniques that emphasize the missing transverse energy ($E_{\rm T}^{\rm miss}$) may no longer be appropriate. Instead, we have developed alternate methods to search for various types of RPV decays. To search for hadronic RPV, which arises when any of the λ''_{ijk} are non-zero, we search in events with zero leptons using the jet and b-tagged jet multiplicities of the event. In this note, the LSP is assumed to decay promptly.

Searches for multijet resonances, a prominent signal when hadronic RPV is present, have been performed by CDF [9], ATLAS [10], and CMS [11–13]. The ATLAS experiment has performed an inclusive hadronic search with a requirement of high jet multiplicity [14]. Searches for RPV interactions in multilepton final states have been carried out at LEP [15–17], the Tevatron [18, 19], at HERA [20, 21], and at the Large Hadron Collider (LHC) [22–27].

In this note, we interpret the results of an all-hadronic search in a model of RPV supersymmetry in which $\lambda''_{323} \neq 0$. This coupling is expected to be the largest R-parity-violating coupling in certain MFV scenarios [8]. The dataset we used corresponds to 19.5^{-1} fb, which was recorded

in 2012 by the CMS detector at the LHC in proton-proton collisions at a center-of-mass energy of 8 TeV.

The paper is organized as follows. Section 2 presents an overview of the CMS detector, and section 3 describes the event selection. A description of simulated signal and background samples is given in section 4. The limit-setting procedure as well as the treatment of signal samples is described in section 5. Section 6 details a search for hadronic RPV in a zero-lepton final state. We then summarize the conclusions of this paper.

2 CMS Detector

A detailed description of the Compact Muon Solenoid detector, together with a definition of the coordinate system used, can be found in Ref. [28]. The central feature of the CMS apparatus is a superconducting solenoid with an internal diameter of 6 m, which generates a 3.8 T uniform magnetic field along the axis of the LHC beams. A silicon pixel and strip tracker, a crystal electromagnetic calorimeter (ECAL) and a brass/scintillator hadron calorimeter (HCAL) are located within the magnet. Muons are identified and measured in gas-based detectors embedded in the outer steel magnetic flux return yoke of the solenoid. In addition to the barrel and endcap detectors, CMS has extensive forward calorimetry. The inner tracker measures charged particles within the pseudorapidity range $|\eta| < 2.5$.

3 Object Selections

Electrons and muons are reconstructed using the tracker, calorimeter, and muon systems. Details of the reconstruction and identification for electrons and muons can be found in Ref. [29] and Ref. [30], respectively. We veto events in which at least one isolated electron or muon has transverse momentum of $p_T > 10\,\text{GeV}$ and $|\eta| < 2.4$.

To ensure that electrons and muon candidates are isolated, we use a particle-flow (PF) algorithm [31, 32] to identify the source of transverse energy deposits in the trackers and calorimeters. We then calculate $E_{T,\text{cone}}$, defined as the sum of transverse energy deposits that are within a cone of radius $\Delta R \equiv \sqrt{(\Delta\eta)^2 + (\Delta\phi)^2} = 0.3$ around the candidate, excluding the candidate itself. We remove energy from additional simultaneous proton-proton collisions by subtracting a per-event correction [29, 33]. Finally, we divide $E_{T,\text{cone}}$ by the lepton p_T to find the relative isolation $I_{\text{rel}} = E_{T,\text{cone}}/p_T$, which is required to be less than 0.15.

We reconstruct jets from PF candidates [33] using the anti-k_T algorithm [34] with a distance parameter of 0.5. Jets are required to have $|\eta| < 2.5$ and $p_T > 50\,\text{GeV}$ and be at least $\Delta R > 0.3$ away from any isolated electron or muon candidate. Jet four-momenta are varied using p_T and η-dependent correction factors [35] to account for the uncertainty in the jet energy scale measurement. The uncertainty in the jet energy resolution is accounted for using p_T and η-dependent data-to-simulation resolution ratios based on the difference between reconstructed and matched generator jet p_T.

To determine if the jet originated from a bottom quark, we use the combined secondary-vertex (CSV) algorithm, which calculates a likelihood discriminant from the track impact parameter and secondary-vertex information [36]. Jets are identified as arising from b-quarks using the combined secondary vertex algorithm with the tight selection ($CSV > 0.898$), corresponding to an average efficiency of 50% for jets arising from b quarks and a false tag rate of 0.1% for light quarks. Scale factors, depending on p_T and $|\eta|$, are measured in data control samples of $\bar{t}t$ and μ+jets events and are used to correct the tagging efficiencies obtained from simulation. A

weight is applied to the response of the b-tagging algorithm for each jet that is matched to a b quark. A similar procedure is applied to model the mistag probability for jets originating from light quarks (u,d,s), c quarks, and gluons.

The b-, c-, and light-flavor quark-tagging efficiencies are varied separately within their statistical uncertainties, and data-to-simulation scale factors are applied and varied within the measured uncertainties [36, 37]. The b and c quark scale factors are treated as correlated, and the light flavor scale factors are treated as uncorrelated with the heavy flavor scale factors.

4 Simulation

Monte Carlo (MC) simulations are used to estimate some of the SM backgrounds and to understand the efficiency and acceptance of the signal model. The SM background samples are generated using MADGRAPH [38] with parton showering and fragmentation modeled using PYTHIA (version 6.420) [39] and passed through a GEANT4-based [40] representation of the CMS detector. Signal samples [41] are generated with MADGRAPH and PYTHIA and passed through the CMS fast-simulation package [42]. The `CTEQ6L1` [43] set of parton distribution functions (PDFs) is used throughout. Cross sections for SUSY signal processes, calculated at next-to-leading-order (NLO) with next-to-leading-log (NLL) resummation, are taken from the LHC SUSY cross sections working group [44–48]. In these calculations, all sparticles except those directly produced are assumed to be decoupled. Background yields, when taken from simulation, are normalized to NLO or next-to-next-to-leading-order (NNLO) cross sections, when available.

5 Procedures for signal samples and limits

This analysis is interpreted in the simplified model scenario (SMS) framework of SUSY [49–51]. In these interpretations, sparticles not explicitly considered are assumed have very large masses so that their effect is negligible. However, the masses of intermediate states are assumed to be small enough that all sparticles decay promptly.

The uncertainty on the knowledge of the parton density functions is obtained applying the prescription of the PDF4LHC working group [52]. Most of the signal samples used in this paper are generated with a fast parameterized MC. Corrections for the ratio of b-tagging efficiencies and light-flavor mistag rates between fast and full simulation are applied as a function of p_{T} and $|\eta|$. Finally, the uncertainty on the modeling of final- and initial-state radiation was obtained from the discrepancies between data and simulation observed in the p_T distributions of Z+jets, dibosons+jets and $\mathrm{t\bar{t}}$+jets events as a function of the p_T of the recoiling system [53].

Limits are calculated from the LHC-style CLs [54, 55] ratio of test statistics, using the formalism developed by the CMS and ATLAS collaborations in the context of the LHC Higgs Combination Group [56]. For each cross section σ under test, the likelihood is profiled with respect to nuisance parameters; that is, nuisance parameters are treated as fit parameters subject to external constraints on their magnitude and distribution. We find the one-sided p-value of the observed data in the signal-plus-background hypothesis, denoted p_σ. This is the fraction of pseudo-experiments with $\lambda_p^{\mathrm{mod}}(\sigma)$ less than the value measured in data. We also generate pseudo-experiments with the signal cross section set to zero to construct the distribution of $\lambda_p^{\mathrm{mod}}(\sigma)$, where σ is the tested cross section value. From these pseudo-experiments we obtain the distribution of the test statistic in the background-only hypothesis, and from this distribution we obtain the p-value of data in the background-only hypothesis, denoted p_0. Then $\mathrm{CL_s}$ is

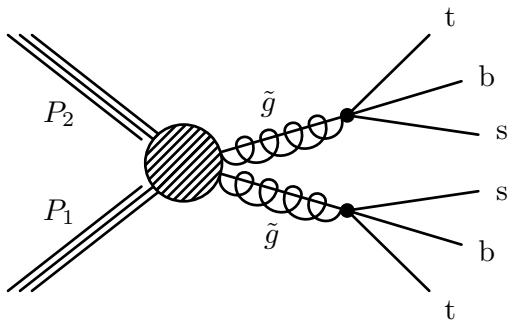

Figure 1: Feynman diagram for pair production of gluinos decaying to tbs.

defined as $p_\sigma/(1-p_0)$. If $CL_s < 0.05$, we reject that σ at 95% confidence level (CL). The largest cross section not rejected corresponds to the the CL_s upper limit.

6 Fully hadronic final state

Many signatures for new physics beyond the standard model result in long decay chains that produce high multiplicity final states. However, most searches for SUSY involve either leptonic final states or missing transverse momentum. Fully hadronic final states that do not result in missing transverse momentum have been explored less thoroughly, and large discrepancies with respect to the standard model could still be present in the data. This section presents a search in a high multiplicity, fully hadronic final state with no missing transverse momentum requirement. The multiplicity of b-tagged jets is used as a discriminating variable.

Results are interpreted in terms of a model in which pair-produced gluinos each decay via $\tilde{g} \to$ tbs, which is allowed when $\lambda''_{332} \neq 0$ so that an antitop squark couples directly to the final state b and s quarks. The top squark is assumed to be heavier than the gluino, resulting in the three-body decay of the gluino shown in Fig. 1. All sparticles other than the top squark and the gluino are considered to be decoupled. The top squark mass and λ''_{332} are assumed to take values such that the gluino decays promptly. Because the coupling λ''_{332} involves heavy quarks, it is relatively unconstrained by measurements of nucleon stability or neutrino masses.

We proceed as follows. We bin the data in the jet multiplicity N_{jet}, and the scalar sum of the transverse momenta of the jets, H_T. In each (N_{jet}, H_T) bin we fit the distribution of the multiplicity of b-tagged jets (N_b) with a probability distribution function comprising a sum of SM and signal components. The sample includes bins that would be free of any signal, used to facilitate the background estimation. The component fit functions are derived from simulation, after corrections based on data where needed. Specifically, the analysis is performed in ten bins of N_{jet} and H_T. The H_T bins are $1.0 < H_T < 1.75$ TeV and $H_T > 1.75$ TeV. and the N_{jet} bins are 4, 5, 6, 7, and ≥ 8. Though the signal has at least ten jets, a looser selection for the highest N_{jet} bin is necessary in order to obtain a non-zero prediction in the $N_b \geq 3$ signal region. The low N_{jet} bins (4–6) are used for validation and control samples, while the $N_{\text{jet}} \geq 8$ bin is the most sensitive signal bin. The contribution of signal to the $N_{\text{jet}} = 4-5$ bins is negligible, and these bins are therefore not included in the fit made to extract the signal.

6.1 Event Selection

Events are selected online via a requirement on H_T that varied between 650 and 750 GeV over the course of the data-taking run.

Substantial background suppression is achieved through the application of multiplicity requirements on the jets reconstructed in the event, together with p_{T} threshold requirements. Specifically, we require four jets with p_{T} >50 GeV, where at least one jet must additionally satisfy p_{T} >150 GeV. The offline H_T of the event, calculated with these jets, is required to be greater than 1.0 TeV. With these selections, the trigger efficiency, measured with prescaled triggers that have lower H_T requirements, is consistent with 100%.

To minimize the contribution of light jet fakes, a tight selection is used to identify jets as arising from b-quarks. At least two such b-tagged jets are required.

Events are required to have no isolated muons or electrons with $p_T > 10$ GeV. This requirement renders backgrounds due to feed-down from leptonic final states essentially negligible.

6.2 Determination of SM background

As the dominant background in this analysis arises from multijet events (QCD), the modeling of the QCD component is crucial. We proceed by deriving corrections from data to the simulated QCD background to predict the distribution of the number of b-tagged jets. There are three main concerns: the modeling of the N_{jet} and H_T distributions, of the flavor composition, and of the b-quark production mechanisms.

The uncertainty in the predicted yield of QCD events arising from the QCD multijet cross section uncertainty is avoided by binning the sample in N_{jet} and H_T. The QCD yield is then determined from a fit to data in each (N_{jet}, H_T) bin with the aid of a third variable, N_b. After normalizing the QCD yield to data in H_T and N_{jet} bins, we require only small corrections to the N_b spectrum.

The choice of a tight b-tagging selection significantly reduces the effect of falsely tagged light jets, and its uncertainty. The flavor composition of the simulated QCD samples is corrected using b-tag efficiency scale factors, with an additional constraint based on a fit of the distribution of the CSV discriminant in a QCD-dominated low N_{jet} sideband (Sect. 6.2.1).

The primary source of uncertainty in the yield of b-tagged jets from true b quarks arises from gluon splitting: $\mathrm{g} \to \mathrm{b\bar{b}}$. Discrepancies between data and MC arise primarily in the region of low $\Delta R_{\mathrm{b\bar{b}}}$, with $\Delta R_{\mathrm{b\bar{b}}}$ taken between the two b-tagged jets [57], where gluon splitting is important. We use the high $\Delta R_{\mathrm{b\bar{b}}}$ region as a normalization sample to determine a gluon splitting systematic uncertainty from the low $\Delta R_{\mathrm{b\bar{b}}}$ region (Sect. 6.2.2).

With this procedure, we obtain a data-driven estimation of the QCD background in the variables N_{jet}, H_T, and N_b.

6.2.1 Flavor composition correction

To ensure that the QCD MC has the appropriate flavor composition, events are reweighted to match the flavor composition seen in data. The coefficients used in the reweighting procedure are derived from a fit to the distribution of the CSV discriminant in a subset of the region of CSV discriminant selected by the b-tagging requirement of this analysis, CSV > 0.9.

The fit of the distribution of the CSV discriminant is performed, including the statistical uncertainty on the MC prediction as nuisance parameters in the fit via the Barlow-Beeston method [58]. To exclude a potential bias from signal contamination, only events with four or five reconstructed jets are included in this fit. Additionally, to avoid bias due to the large weights arising from the low equivalent luminosity of the simulated QCD samples with low H_T, the H_T requirement is increased slightly to $H_T > 1.1$ TeV; it has been verified that the flavor compo-

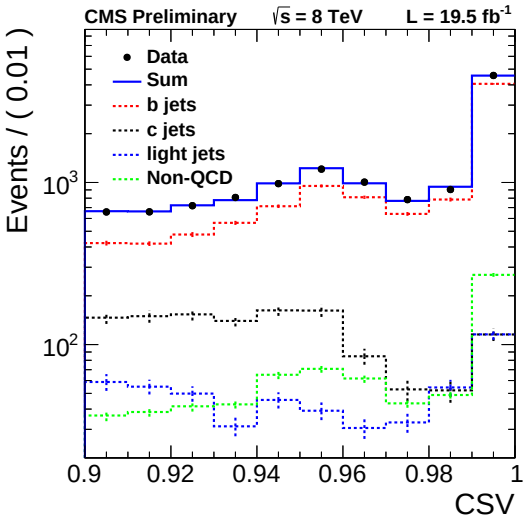

Figure 2: Fit to the CSV distribution in data for $4 \leq N_{\text{jet}} \leq 5$, $H_T > 1.1$ TeV and CSV > 0.9. Error bars indicate the statistical uncertainty arising from MC statistics.

sition corrections are statistically identical for requirements of 1.0 or 1.1 TeV. First, the overall QCD contribution is normalized to the data yield minus the expected non-QCD yield. Next, reconstructed jets are matched to the corresponding MC jet, and templates for the CSV discriminant are formed for each flavor. Then the relative normalization of templates corresponding to truth-matched bottom and charm jets are allowed to vary in the fit. The small contributions of non-QCD events (mainly $\mathrm{t\bar{t}}$) and light flavor QCD jets are fixed in the fit, though the uncertainty on the light flavor fraction is considered as a systematic uncertainty.

The fractions of bottom, charm and light flavor jets prior to the fit are f_b, f_c, and f_{light}, respectively. The fit provides new fractions f_i' defined as

$$f_i' = \frac{n_i}{n_b + n_c + n_{\text{light}} + n_{\text{non-QCD}}} \tag{2}$$

where n_b and n_c are the fitted yields of bottom and charm jets, respectively; n_{light} and $n_{\text{non-QCD}}$ are the fixed light quark and non-QCD yields. The index i refers to one of the contributions in the denominator. The fitted f_i' are listed in Table 1 and the fit of the CSV distribution is shown in Fig. 2. The fit quality is good, with χ^2/ndof=7.0/6, providing confidence in the modeling of the CSV distributions.

For each event, a weight is assigned based on the flavor fractions

$$w_{\text{event}} = \prod_{\text{b-jet}} w_{\text{b-jet}}(\text{flavor}) \tag{3}$$

where $w_{\text{b-jet}} = f'_{\text{flavor}}/f_{\text{flavor}}$ is a per-jet weight. This form of the per-event reweighting is motivated by treating the corrections as independent corrections to the per-jet efficiency.

Though the fit models the data well, the good agreement between the model and the data could occur if mismodeled distributions accidentally have a linear combination that is consistent with the data. To eliminate this possibility, fits are performed with variations of the fit range. Even with an extreme variation in which the most sensitive region of the fit (CSV > 0.98) is removed, the fit results are still consistent with the nominal fit. There is no evidence for any systematic effect.

As an additional cross-check, the fit is iterated: after the simulated events have been reweighted, the reweighted templates are fit to the data again. All three of the resulting weights are consistent with 1.0, to within 1σ, as shown in Table 1.

Table 1: Reweighting fractions $f_{b,c,\text{light}}$ derived from the fit of the low N_{jet} control region before and after reweighting the QCD MC.

Flavor	Before reweighting	After reweighting
b	0.94 ± 0.03	1.02 ± 0.03
c	1.99 ± 0.43	0.84 ± 0.18
light	fixed to 1.0	fixed to 1.0

It is important that the weights derived in this fit of the $N_{\text{jet}} = 4 - 5$ sideband are applicable to the $N_{\text{jet}} \geq 6$ signal regions. This has been verified in two ways. First, the weights have been applied to the signal-depleted $N_{\text{jet}} = 6$ region. The corrected predictions show good agreement with the data, as seen in Fig. 3. Second, as the expected signal yield is extremely small compared to the background in the region defined by $H_T > 1.1$ TeV, $N_b \geq 2$, and $N_{\text{jet}} \geq 6$, the CSV distribution can be fit directly in this region. The reweighting parameters resulting from this fit are all within 1σ of those from the low-N_{jet} sideband. The fit of the high N_{jet} region is not used in the reweighting procedure due to the poorer statistical uncertainty it provides on the derived weights as well as due to the small but unknown potential bias due to signal contamination.

6.2.2 Gluon-splitting systematic uncertainty

Jets containing b quarks are produced in three different ways: pair production ($q\bar{q} \to b\bar{b}$), flavor excitation ($bq \to bq$ and charge conjugate), and gluon splitting ($g \to b\bar{b}$). The first two processes are important primarily in the initial hard scatter, and the second is suppressed due to the small intrinsic b-quark content of the proton. Pair production is known to be well-modeled by MADGRAPH MC, but the rate of gluon splitting is known to be off by up to about a factor of two [57], necessitating a data-driven systematic uncertainty.

The different b-quark production mechanisms result in different angular distributions between the two produced b-quarks. The gluon splitting correction is determined using the $\Delta R_{b\bar{b}}$ distribution, where $\Delta R_{b\bar{b}}$ is computed between any two b-tagged jets in the event. This distribution, shown in Fig. 4, is normalized in the high $\Delta R_{b\bar{b}}$ region, $\Delta R_{b\bar{b}} \geq 2.4$. The difference between data and MC in $\Delta R_{b\bar{b}} \leq 1.6$ is assumed to arise entirely from gluon splitting to $b\bar{b}$ pairs.

A contribution of truth-matched gluon splitting events, normalized to the data-MC difference in the yield in the low $\Delta R_{b\bar{b}}$ region, is added to the QCD prediction. The QCD histograms that are input to the systematic variation templates in the fit are determined by normalizing the QCD contribution to its LO cross section, then multiplying by the normalization determined in the high ΔR region, and then adding the gluon splitting contribution. The final normalization of the QCD background is determined in the fit. The constraint on the modeling of gluon splitting at low $\Delta R_{b\bar{b}}$ is used as uncertainty rather than a correction because in the large N_{jet} regions statistical fluctations at low $\Delta R_{b\bar{b}}$ are larger than the effect that it would correct.

6.2.3 Hadronic decays of electroweak bosons

Though the background to this analysis is dominated by QCD and $t\bar{t}$ decays, hadronic W and Z bosons decays can contribute as well. These backgrounds are very small, but it is necessary to take them into account as they can be enriched in heavy flavor (either due to $W \to c\bar{s}$ or $Z \to b\bar{b}$). To predict the background due to hadronic decays of W and Z bosons, hadronic

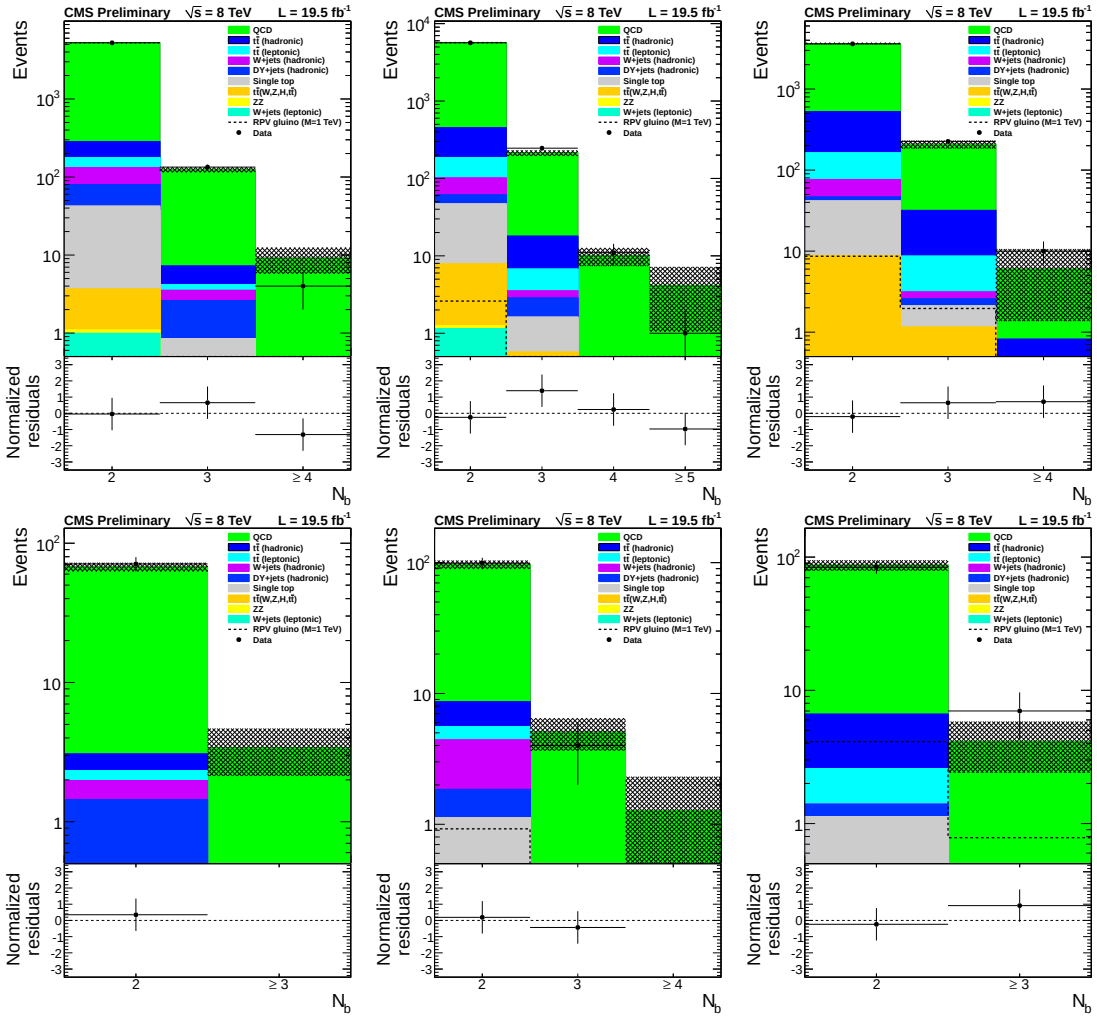

Figure 3: Data (dots with error bars) and the corrected prediction of the N_b distribution are shown. The shaded band shows the MC statistical uncertainty. The top (bottom) row shows data in which events are required to have $1000 < H_T < 1750$ GeV ($H_T > 1750$ GeV). The jet multiplicity requirements are $N_{\text{jet}} = 4$ (left), $N_{\text{jet}} = 5$ (middle), and $N_{\text{jet}} = 6$ (right).

decays are emulated with simulated data samples in which the W boson or Z boson decays leptonically, treating the leptons in the boson decays as quarks. In both cases, if a lepton is within the jet acceptance ($p_{\text{T}} > 50$ GeV and $|\eta| < 2.4$) and is separated by more than $\Delta R = 0.5$ from other jets, it is treated as a quark and added to N_{jet} and H_T. The quark is considered to be a b-tagged quark according to the probability provided by the b-tag efficiency parameterization. If the emulated candidate passes this accept-reject procedure, it is considered a b-tagged jet and N_b is incremented as well.

The total background due to hadronic W and Z decays are each less than 1% in all signal regions.

6.3 Systematic uncertainties

Systematic uncertainties due to the modeling of QCD background constitute an important part of the total uncertainty. The uncertainty due to the gluon splitting is modeled by considering fits in which the gluon splitting rate determined from the low $\Delta R_{\text{b}\bar{\text{b}}}$ region is used as a

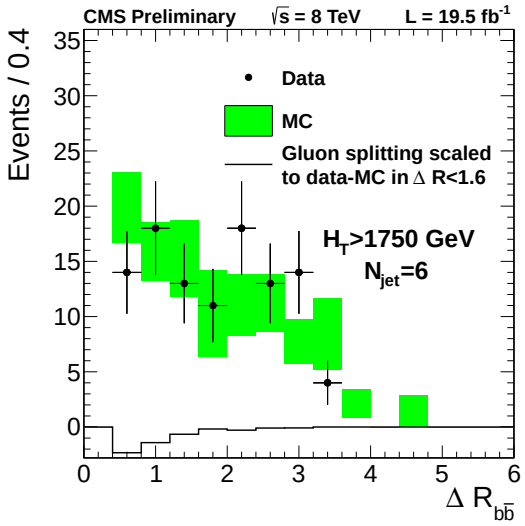

Figure 4: Data (dots with error bars), uncorrected MC prediction (band), and truth-matched gluon splitting events scaled to the data-MC difference in $\Delta R < 1.6$ (histogram) in a typical signal region corresponding to $H_T > 1750$ GeV and $N_{\text{jet}} = 6$.

correction.

As $t\bar{t}$ is a sub-dominant background, the effect of its uncertainties are generally small. The tune of the underlying event, as well as variations of the renormalization, factorization, and matching scales are considered. Also, the inclusive $t\bar{t}$ production cross section is varied according to its NNLO+NNLL uncertainty [59]. The top quark p_{T} spectrum is reweighted to agree with its NNLO prediction and with the data.

The cross-sections of sub-leading backgrounds are varied by 50 percent, and the luminosity is varied according to its uncertainty of 2.6%.

Since the trigger efficiency is consistent with 100% no uncertainty is assigned for trigger efficiency.

The QCD MC is affected by large statistical uncertainties, which are taken into account by variations in which a single bin of each (N_{jet}, H_T) histogram is varied according to its statistical uncertainty. The largest systematic uncertainty in most N_b bins is due to the statistical uncertainty on the templates from the small equivalent luminosity of the QCD MC samples.

Systematic uncertainties are summarized in Table 2.

6.4 Control sample fit

Signal-depleted control regions at low N_{jet} (N_{jet} =4, 5, and 6) are studied before examining the signal region. For low jet multiplicities, $t\bar{t}$ backgrounds are less important, giving a largely pure sample of QCD.

A binned maximum likelihood fit is performed in which systematic uncertainties are profiled. Systematic uncertainties are included as shape uncertainties by interpolating between histograms corresponding to $\pm 1\sigma$ variations. As the H_T and N_{jet} dependence of the QCD contribution may not be modeled well by leading-order QCD MC, a separate normalization of the QCD contributions is allowed in each bin of H_T and N_{jet}. The likelihood used in the fit of the

Table 2: Systematic uncertainties, in percent. The entries in the table are formated as $N_{\text{jet}} = 6/N_{\text{jet}} = 7/N_{\text{jet}} \geq 8$.

Systematic	$1.0 < H_T < 1.75$ TeV			$H_T > 1.75$ TeV	
	$N_b = 2$	$N_b = 3$	$N_b \geq 4$	$N_b = 2$	$N_b \geq 3$
b,c jet b-tag SF	0.24/0.24/0.32	4/3.4/2.9	3.7/5.6/5.9	0.56/0.26/0.32	12/6.3/4.6
u,d,s jet b-tag SF	0.05/0.028/0.0079	0.48/0.38/0.073	14/0.81/0.12	0.011/0.005/0.034	0.23/0.12/0.49
Tune ($t\bar{t}$)	0.09/0.027/0.18	1.5/0.58/2.6	1.4/2.9/8.8	0.085/0.48/0.81	1.8/12/12
Matching ($t\bar{t}$)	0.078/0.11/0.39	0.81/2.5/3.5	20/14/7	0.071/1.5/2.4	1.5/36/35
Scale ($t\bar{t}$)	0.025/0.43/0.97	0.58/5.9/9.9	4.8/12/2.9	0.44/1.1/2.2	9.3/26/32
p_T ($t\bar{t}$)	0.073/0.17/0.38	1.2/2.5/3.5	1.9/1.8/7	0.03/0.023/0.013	0.63/0.55/0.19
$t\bar{t}b\bar{b}$ yield	0.19/0.47/1.5	3.1/6.6/13	3.9/10/29	0.19/0.016/0.66	4.1/0.4/9.4
σ ($t\bar{t}$)	0.00052/0.0048/0.014	0.01/0.046/0.12	0.031/0.47/0.27	0.0045/0.0032/0.03	0.094/0.077/0.44
σ minor bkg.	0.015/0.041/0.13	0.27/0.61/1.2	0.41/0.21/1.5	0.019/0.042/0.0043	0.41/1/0.062
Jet p_T scale	0.47/0.45/0.94	7.3/7/9.6	28/2.9/2.5	0.31/0.31/0.66	6.6/7.5/9.4
Jet resolution	0.39/0.095/0.69	6.5/2.1/5.3	10/11/25	0.042/0.19/0.44	0.88/4.6/6.4
Gluon splitting	0.15/1.1/0.27	2.3/16/2.8	10/0.42/0.88	0.34/0.13/0.11	7.2/3/1.5
b-jet reweighting stat.	0.0021/0.023/0.027	0.11/0.12/0.56	2.5/4.1/3.7	0.21/0.24/0.19	4.5/5.8/2.7
c-jet reweighting stat.	0.053/0.0072/0.21	0.99/0.39/2.5	1.8/5/3.5	0.3/0.28/0.34	6.3/6.8/4.8
Pileup	0.15/0.53/0.17	2.4/8.4/1.6	8.8/6.4/1.9	0.28/0.56/0.056	5.9/14/0.81
Total (excl. QCD MC stat.)	0.73/1.5/2.3	12/22/21	41/26/41	0.99/2.1/3.6	21/50/51
QCD MC statistics	2.5/3.7/5.6	11/14/14	77/54/35	9/10/13	42/37/43
Statistical	1.7/2.5/4	6.9/9.9/13	41/42/47	11/14/18	49/70/68

signal and control regions is

$$N_{\text{norm}} \left[\prod_{i \in H_T \text{ bins}} \prod_{j \in N_{\text{jet}} \text{ bins}} \left(\text{Poisson}(N_{ij} | \mu_{\text{signal}} \nu_{ij,\text{signal}} + \mu_{ij,\text{QCD}} \nu_{ij,\text{QCD}} + \nu_{ij,\text{other}}) \right) \right] \prod_{k \in \text{syst}} P(N_{ij} | \theta_k) \tag{4}$$

Here μ_{signal} and $\mu_{ij,\text{QCD}}$ are H_T and N_{jet}-dependent normalization constants. The QCD and non-QCD backgrounds are relative to nominal values specified by $\nu_{ij,\text{QCD}}$ and $\nu_{ij,\text{other}}$, respectively. The control sample fit is based on the data and MC shown in Fig. 3. In this fit, the product over N_{jet} bins is restricted to N_{jet} =4, 5, 6, and the signal yields are fixed to zero.

All of the nuisance parameters are consistent within $\pm 1\sigma$ of their pre-fit uncertainties, except for a 1.4σ discrepancy in the light jet fraction nuisance parameter, which is however a subdominant uncertainty in the high N_{jet} signal region.

6.5 Signal efficiency and systematics

Several of the systematic uncertainties affecting the signal yield are evaluated in the same way as the background yield. These are the jet p_{T} scale, the heavy flavor b-tag scale factors and the light flavor b-tag scale factors.

The signal samples are generated with a fast parameterized simulation. The efficiency after all selections is shown in Fig. 6 (left) and achieves a maximum value of 22% for $m_{\text{gluino}} = 1$ TeV. Nuisance parameters corresponding to $\pm 1\sigma$ variations on the uncertainty of these corrections for bottom jets, charm jets, and light-flavor jets are considered separately and assumed to be mutually uncorrelated.

PDF uncertainties are evaluated according to the PDF4LHC recommendation [52].

In all signal regions the PDF uncertainty dominates the overall uncertainty on the acceptance times efficiency and reaches up to 32% in the signal region with $H_T > 1.75$ and $N_{\text{jet}} \geq 8$. All signal systematic uncertainties are modeled as templates, with the exception of the PDF uncertainty, which is modeled as a lognormal constraint for each (N_{jet}, H_T) bin.

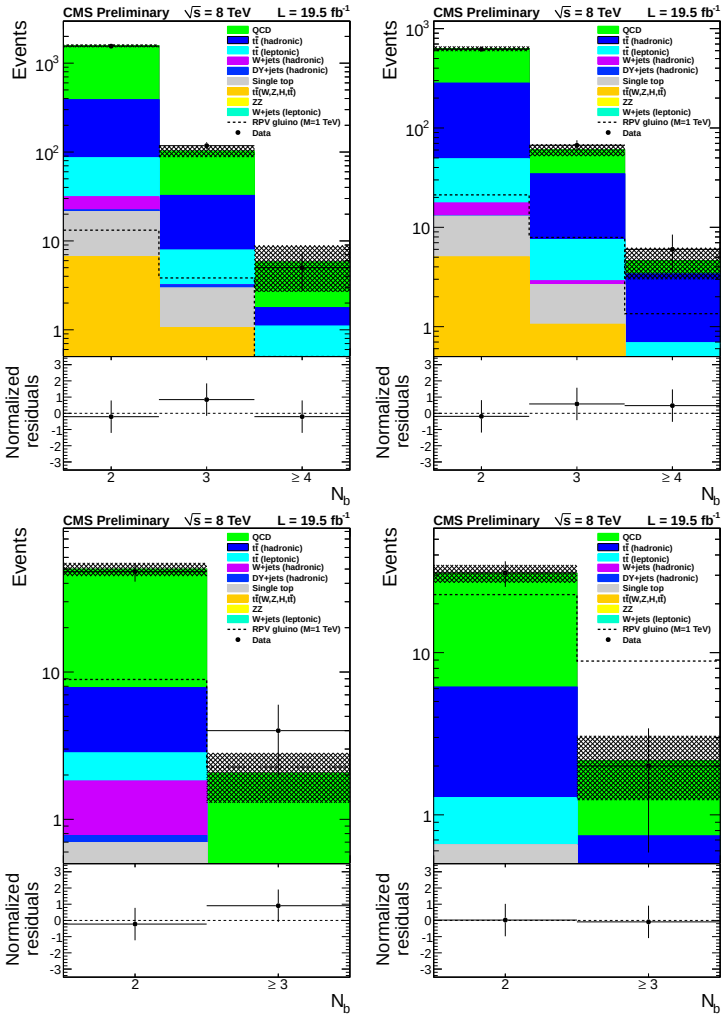

Figure 5: Data (dots with error bars) and the corrected prediction of the N_b distribution in the high N_{jet} signal region. The shaded band shows the MC statistical uncertainty. The top (bottom) row shows data in which events are required to have $1000 < H_T < 1750$ GeV ($H_T > 1750$ GeV). The jet multiplicity requirements are $N_{\text{jet}} = 7$ (left) and $N_{\text{jet}} \geq 8$ (right).

6.6 Results and interpretation

The likelihood used in the fit of the signal region is that given by Eq. 4, with the N_{jet} product spanning $N_{\text{jet}} = 6, 7, 8$, and with μ_{signal} left free. Figure 5 shows a comparison of the data with the corrected MC, where the QCD component has been scaled to the data yield minus the non-QCD background yields obtained from MC.

At each gluino mass, the best fit is zero events. Figure 6 (right) shows the expected and observed limits compared to the gluino pair production cross section.

In conclusion, the data in the signal regions are well described by the background predictions. The results are interpreted in terms of a specific model of R-parity-violating supersymmetry in which gluinos are pair produced and each gluino decays promptly via $\tilde{g} \to tbs$. Cross section limits are calculated and result in a 95% CL lower limit on the gluino mass of 0.98 TeV within this simplified model.

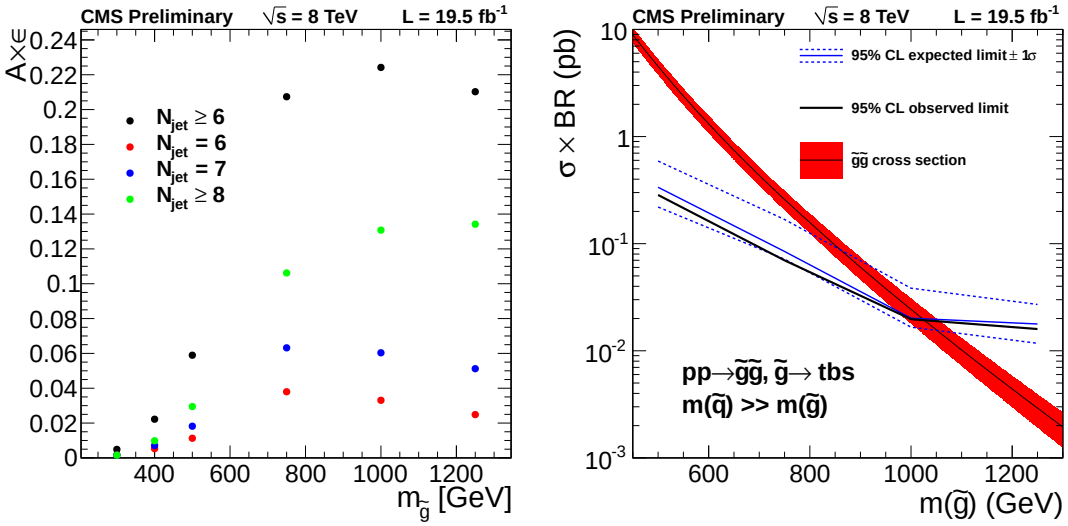

Figure 6: Signal efficiencies as a function of $m_{\tilde{g}}$ for $N_b \geq 2$, $H_T > 1.0$ TeV, and $N_{\text{jet}} \geq 6$, together with the breakdown among N_{jet} bins (left). Expected and observed limits in the all-hadronic $\tilde{g} \to$ tbs analysis. The red band is the gluino pair production cross section (right).

7 Summary

This paper explores a fully hadronic final state in which R-parity-violating supersymmetry could appear. In $19.3 - 19.5\,\text{fb}^{-1}$ of CMS data collected in 2012 at $\sqrt{s}$=8 TeV, we find no discrepancies relative to standard-model expectations. In a model that explores the consequences of minimal flavor violation, we use the b-tagged and total jet multiplicity distributions to set limits on the mass of a gluino that decays via λ''_{332} to a top, bottom, and strange quark. We exclude gluinos with masses less than 0.98 TeV at 95% CL.

References

[1] H. P. Nilles, "Supersymmetry, Supergravity and Particle Physics", *Phys. Rept.* **110** (1984) 1, doi:10.1016/0370-1573(84)90008-5.

[2] H. E. Haber and G. L. Kane, "The Search for Supersymmetry: Probing Physics Beyond the Standard Model", *Phys. Rept.* **117** (1985) 75, doi:10.1016/0370-1573(85)90051-1.

[3] G. R. Farrar and P. Fayet, "Phenomenology of the production, decay, and detection of new hadronic states associated with supersymmetry", *Phys. Lett. B* **76** (1978) 575, doi:10.1016/0370-2693(78)90858-4.

[4] R. Barbier et al., "R-parity violating supersymmetry", *Phys. Rept.* **420** (2005) 1, doi:10.1016/j.physrep.2005.08.006, arXiv:hep-ph/0406039.

[5] Particle Data Group, J. Beringer et al., "Review of Particle Physics (RPP)", *Phys. Rev. D* **86** (2012) 010001, doi:10.1103/PhysRevD.86.010001.

[6] A. Y. Smirnov and F. Vissani, "Upper bound on all products of R-parity violating couplings lambda-prime and lambda-prime-prime from proton decay", *Phys.Lett.* **B380** (1996) 317–323, doi:10.1016/0370-2693(96)00495-9, arXiv:hep-ph/9601387.

[7] E. Nikolidakis and C. Smith, "Minimal Flavor Violation, Seesaw, and R-parity", *Phys.Rev.* **D77** (2008) 015021, doi:10.1103/PhysRevD.77.015021, arXiv:0710.3129.

[8] C. Csaki, Y. Grossman, and B. Heidenreich, "MFV SUSY: A Natural Theory for R-Parity Violation", *Phys. Rev. D* **85** (2012) 095009, doi:10.1103/PhysRevD.85.095009, arXiv:1111.1239.

[9] CDF Collaboration, "First Search for Multijet Resonances in $\sqrt{s} = 1.96$ TeV $p\overline{p}$ Collisions", *Phys. Rev. Lett.* **107** (2011) 042001, doi:10.1103/PhysRevLett.107.042001, arXiv:1105.2815.

[10] ATLAS Collaboration, "Search for pair production of massive particles decaying into three quarks with the ATLAS detector in $\sqrt{s} = 7$ TeV pp collisions at the LHC", *JHEP* **12** (2012) 086, doi:10.1007/JHEP12(2012)086, arXiv:1210.4813.

[11] CMS Collaboration, "Search for three-jet resonances in pp collisions at $\sqrt{s} = 7$ TeV", *Phys. Lett. B* **718** (2012) 329, doi:10.1016/j.physletb.2012.10.048, arXiv:1208.2931.

[12] CMS Collaboration, "Search for Three-Jet Resonances in pp Collisions at $\sqrt{s} = 7$ TeV", *Phys. Rev. Lett.* **107** (2011) 101801, doi:10.1103/PhysRevLett.107.101801, arXiv:1107.3084.

[13] CMS Collaboration, "Searches for light- and heavy-flavour three-jet resonances in pp collisions at $\sqrt{s} = 8$ TeV", *Phys. Lett. B* **730** (2014) 193–214, doi:10.1016/j.physletb.2014.01.049, arXiv:1311.1799.

[14] ATLAS Collaboration, "Search for massive supersymmetric particles decaying to many jets using the ATLAS detector in pp collisions at $\sqrt{s} = 8$ TeV", *Phys. Rev.* **D91** (2015), no. 11, 112016, doi:10.1103/PhysRevD.91.112016, arXiv:1502.05686.

[15] ALEPH Collaboration, "Search for supersymmetric particles with R-parity violating decays in e^+e^- collisions at $\sqrt{s}$ up to 209 GeV", *Eur. Phys. J. C* **31** (2003) 1, doi:10.1140/epjc/s2003-01311-5, arXiv:hep-ex/0210014.

[16] DELPHI Collaboration, "Search for supersymmetric particles assuming R-parity nonconservation in e^+ e^- collisions at $\sqrt{s}$ = 192 GeV to 208 GeV", *Eur. Phys. J. C* **36** (2004) 1, doi:10.1140/epjc/s2004-01881-6, arXiv:hep-ex/0406009.

[17] L3 Collaboration, "Search for R parity violating decays of supersymmetric particles in e^+e^- collisions at LEP", *Phys. Lett. B* **524** (2002) 65, doi:10.1016/S0370-2693(01)01367-3, arXiv:hep-ex/0110057.

[18] D0 Collaboration, "Search for R-parity violating supersymmetry via the $LL\overline{E}$ couplings λ_{121}, λ_{122} or λ_{133} in $p\bar{p}$ collisions at $\sqrt{s}$ = 1.96 TeV", *Phys. Lett.* **B638** (2006) 441, doi:10.1016/j.physletb.2006.05.077.

[19] CDF Collaboration, "Search for anomalous production of multilepton events in $p\bar{p}$ collisions at $\sqrt{s}$ = 1.96 TeV", *Phys. Rev. Lett.* **98** (2007) 131804, doi:10.1103/PhysRevLett.98.131804, arXiv:0706.4448.

[20] H1 Collaboration, "A search for squarks of Rp-violating SUSY at HERA", *Z. Phys. C* **71** (1996) 211, doi:10.1007/BF02906978, arXiv:hep-ex/9604006.

[21] ZEUS Collaboration, "Search for stop production in R-parity-violating supersymmetry at HERA", *Eur. Phys. J. C* **50** (2007) 269, doi:10.1140/epjc/s10052-007-0240-8, arXiv:hep-ex/0611018.

[22] CMS Collaboration, "Search for Physics Beyond the Standard Model Using Multilepton Signatures in pp Collisions at $\sqrt{s} = 7$ TeV", *Phys. Lett. B* **704** (2011) 411, doi:10.1016/j.physletb.2011.09.047, arXiv:1106.0933.

[23] CMS Collaboration, "Search for anomalous production of multilepton events in pp collisions at $\sqrt{s} = 7$ TeV", *JHEP* **06** (2012) 169, doi:10.1007/JHEP06(2012)169, arXiv:1204.5341.

[24] ATLAS Collaboration, "Search for R-parity-violating supersymmetry in events with four or more leptons in $\sqrt{s} = 7$ TeV pp collisions with the ATLAS detector", *JHEP* **12** (2012) 124, doi:10.1007/JHEP12(2012)124, arXiv:1210.4457.

[25] ATLAS Collaboration, "Search for a heavy narrow resonance decaying to $e\mu$, $e\tau$, or $\mu\tau$ with the ATLAS detector in $\sqrt{s} = 7$ TeV pp collisions at the LHC", *Phys.Lett.* **B723** (2013) 15–32, doi:10.1016/j.physletb.2013.04.035, arXiv:1212.1272.

[26] CMS Collaboration, "Search for top squarks in R-parity-violating supersymmetry using three or more leptons and b-tagged jets", *Phys. Rev. Lett.* **111** (2013) 221801, doi:10.1103/PhysRevLett.111.221801, arXiv:1306.6643v2.

[27] ATLAS Collaboration, "Search for supersymmetry in events with four or more leptons in $\sqrt{s} = 8$ TeV pp collisions with the ATLAS detector", arXiv:1405.5086.

[28] CMS Collaboration, "The CMS experiment at the CERN LHC", *JINST* **3** (2008) S08004, doi:10.1088/1748-0221/3/08/S08004.

[29] CMS Collaboration, "Electron Reconstruction and Identification at $\sqrt{s} = 7$ TeV", CMS Physics Analysis Summary CMS-PAS-EGM-10-004, 2010.

[30] CMS Collaboration, "Performance of CMS muon reconstruction in pp collision events at $\sqrt{s} = 7$ TeV", *JINST* **7** (2012) P10002, doi:10.1088/1748-0221/7/10/P10002, arXiv:1206.4071.

[31] CMS Collaboration, "Study of tau reconstruction algorithms using pp collisions data collected at $\sqrt{s} = 7$ TeV", CMS Physics Analysis Summary CMS-PAS-PFT-10-004, 2010.

[32] CMS Collaboration, "CMS Strategies for tau reconstruction and identification using particle-flow techniques", CMS Physics Analysis Summary CMS-PAS-PFT-08-001, 2009.

[33] CMS Collaboration, "Commissioning of the Particle-Flow Reconstruction in Minimum-Bias and Jet Events from pp Collisions at 7 TeV", CMS Physics Analysis Summary CMS-PAS-PFT-10-002, 2010.

[34] M. Cacciari, G. P. Salam, and G. Soyez, "The anti-k_t jet clustering algorithm", *JHEP* **04** (2008) 063, doi:10.1088/1126-6708/2008/04/063, arXiv:0802.1189.

[35] CMS Collaboration, "Determination of jet energy calibration and transverse momentum resolution in CMS", *JINST* **06** (November, 2011) 11002, doi:10.1088/1748-0221/6/11/P11002, arXiv:1107.4277.

[36] CMS Collaboration, "Identification of b-quark jets with the CMS experiment", *JINST* **8** (2013) P04013, doi:10.1088/1748-0221/8/04/P04013, arXiv:1211.4462.

[37] CMS Collaboration, "Performance of b-tagging at $\sqrt{s} = 8$ TeV in multijet, $t\bar{t}$ and boosted topology events", CMS Physics Analysis Summary CMS-PAS-BTV-13-001, 2013.

[38] F. Maltoni and T. Stelzer, "MadEvent: automatic event generation with MadGraph", *JHEP* **02** (2003) 027, doi:10.1088/1126-6708/2003/02/027, arXiv:hep-ph/0208156.

[39] T. Sjöstrand, S. Mrenna, and P. Z. Skands, "A brief introduction to PYTHIA 8.1", *Comput. Phys. Commun.* **178** (2008) 852, doi:10.1016/j.cpc.2008.01.036, arXiv:0710.3820.

[40] GEANT4 Collaboration, "GEANT4—a simulation toolkit", *Nucl. Instrum. Meth. A* **506** (2003) 250, doi:10.1016/S0168-9002(03)01368-8.

[41] J. A. Evans and Y. Kats, "LHC coverage of RPV MSSM with light stops", *JHEP* **04** (2013) 028, doi:10.1007/JHEP04(2013)028, arXiv:1209.0764.

[42] CMS Collaboration, "The fast simulation of the CMS detector at LHC", *J.Phys.Conf.Ser.* **331** (2011) 032049, doi:10.1088/1742-6596/331/3/032049.

[43] J. Pumplin et al., "New generation of parton distributions with uncertainties from global QCD analysis", *JHEP* **07** (2002) 012, doi:10.1088/1126-6708/2002/07/012, arXiv:hep-ph/0201195.

[44] W. Beenakker et al., "Production of charginos, neutralinos, and sleptons at hadron colliders", *Phys. Rev. Lett.* **83** (1999) 3780, doi:10.1103/PhysRevLett.83.3780, arXiv:hep-ph/9906298.

[45] A. Kulesza and L. Motyka, "Threshold resummation for squark-antisquark and gluino-pair production at the LHC", *Phys. Rev. Lett.* **102** (2009) 111802, doi:10.1103/PhysRevLett.102.111802, arXiv:0807.2405.

[46] A. Kulesza and L. Motyka, "Soft gluon resummation for the production of gluino-gluino and squark-antisquark pairs at the LHC", *Phys. Rev. D* **80** (2009) 095004, doi:10.1103/PhysRevD.80.095004, arXiv:0905.4749.

[47] W. Beenakker et al., "Soft-gluon resummation for squark and gluino hadroproduction", *JHEP* **12** (2009) 041, doi:10.1088/1126-6708/2009/12/041, arXiv:0909.4418.

[48] W. Beenakker et al., "Squark and gluino hadroproduction", *Int. J. Mod. Phys. A* **26** (2011) 2637, doi:10.1142/S0217751X11053560, arXiv:1105.1110.

[49] N. Arkani-Hamed et al., "MARMOSET: The Path from LHC Data to the New Standard Model via On-Shell Effective Theories", arXiv:hep-ph/0703088.

[50] J. Alwall, P. Schuster, and N. Toro, "Simplified Models for a First Characterization of New Physics at the LHC", *Phys. Rev.* **D79** (2009) 075020, doi:10.1103/PhysRevD.79.075020, arXiv:0810.3921.

[51] LHC New Physics Working Group Collaboration, "Simplified Models for LHC New Physics Searches", *J.Phys.* **G39** (2012) 105005, doi:10.1088/0954-3899/39/10/105005, arXiv:1105.2838.

[52] M. Botje et al., "The PDF4LHC Working Group Interim Recommendations", arXiv:1101.0538.

[53] CMS Collaboration, "Search for top-squark pair production in thex single-lepton final state in pp collisions at $\sqrt{s} = 8$ TeV", arXiv:1308.1586.

[54] T. Junk, "Confidence level computation for combining searches with small statistics", *Nucl. Instrum. Meth. A* **434** (1999) 435–443, doi:10.1016/S0168-9002(99)00498-2, arXiv:hep-ex/9902006.

[55] A. L. Read, "Presentation of search results: the CL_s technique", *J. Phys. G* **28** (2002) 2693, doi:10.1088/0954-3899/28/10/313.

[56] LHC Higgs Combination Group, the ATLAS Collaboration, and the CMS Collaboration, "Procedure for the LHC Higgs boson search combination in Summer 2011", Technical Report ATL-PHYS-PUB-2011-11, CMS-NOTE-2011-005., 2011.

[57] CMS Collaboration, "Measurement of $B\overline{B}$ angular correlations based on secondary vertex reconstruction at $\sqrt{s} = 7$ TeV", *JHEP* **136** (2011) 1103, doi:10.1007/JHEP03(2011)136, arXiv:1102.3194.

[58] R. Barlow and C. Beeston, "Fitting using finite Monte Carlo samples", *Comput. Phys. Commun.* **77** (1993) 219, doi:10.1016/0010-4655(93)90005-W.

[59] M. Czakon, P. Fiedler, and A. Mitov, "The total top quark pair production cross-section at $\mathcal{O}(\alpha_S^4)$", *Phys. Rev. Lett.* **110** (2013) 252004, doi:10.1103/PhysRevLett.110.252004, arXiv:1303.6254.